

Development of PARP-1 inhibitors for Breast cancer therapy: *In-silico* scrutinising of potent phytochemicals

Monika Kumari^{1,2}, Brijesh Rathi², Geeta Singh^{1*}

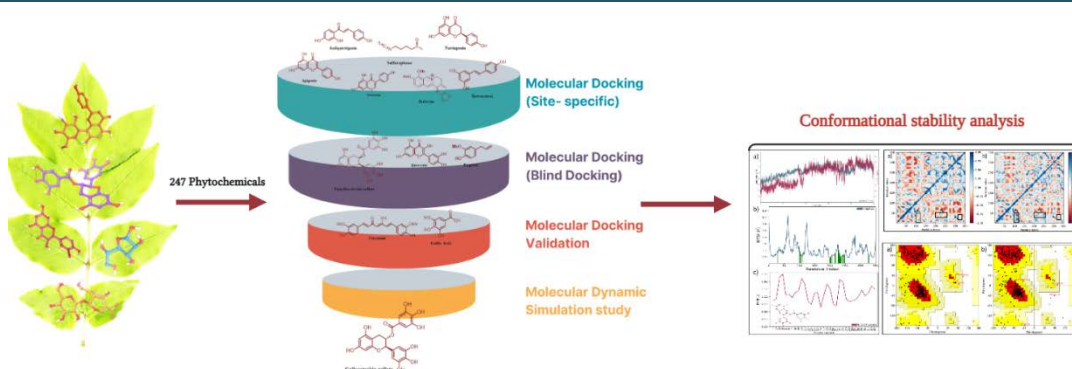
¹Biomedical Engineering Department, Deenbandhu Chhotu Ram University of Science and Technology, Murthal Sonapat, Haryana – 131039 India. ²H. G. Khorana Center For Chemical Biology, Department of Chemistry, Hansraj College, University of Delhi, Delhi – 110007 India

Submitted on: 24-Nov-2024, Accepted and Published on: 02-Jan-2025

Article

ABSTRACT

Breast cancer continues to be the most common cancer globally and a major contributor to cancer-related mortality. Although progress has been made in treatment, considerable challenges remain due to the intricate interplay of various signaling



pathways, transcription factors, and tumor suppressor genes. Current therapies, including chemotherapy, radiotherapy, and targeted therapies, often come with limitations such as toxicity and immune suppression highlighting the need for safer and more effective alternatives. Phytochemicals offer a promising approach due to their low toxicity and anticancer properties. Among key therapeutic targets, poly (ADP-ribose) polymerase-1 (PARP-1) plays a pivotal role in DNA repair and maintaining genomic stability, particularly in breast cancers with BRCA1/2 mutations. Although PARP inhibitors are approved for BRCA-mutated cancers, adverse effects, and resistance necessitate the exploration of natural alternatives. This study investigated the PARP-1 inhibitory potential of phytochemicals targeting the 7KK6 protein structure of active PARP-1. An in-silico screening of 247 phyto-ligands identified lead compounds with strong PARP-1 binding affinity. Molecular dynamics (MD) simulations validated the stability of these complexes, supported by stereochemical and ADME analyses to confirm drug-likeness and bioavailability. Notably, Gallicocatechin gallate (P1) exhibited a superior docking score (-11.574) and binding energy (-81.29 kcal/mol) compared to the control, Veliparib (-8.309, -67.69 kcal/mol). These results highlight Gallicocatechin gallate as a promising PARP-1 inhibitor with potential for breast cancer therapy. Further in-vitro and in-vivo studies are essential to evaluate its clinical efficacy.

Keywords: Breast cancer, molecular docking, phytochemicals, molecular dynamics, PARP-1inhibitor, anti-cancer

INTRODUCTION

Breast cancer is the most widespread cancer worldwide and continues to be a major cause of cancer-associated fatalities in both men and women. According to the 2022 reports from the International Agency for Research on Cancer (IARC), breast cancer accounted for approximately 2.3 million cases, representing about 11.6% of all cancer cases and causing over 670,000 deaths (6.9%).¹

The American Cancer Society estimated that in the United States alone, there will be 2,001,140 new cancer cases and 611,720 cancer-related deaths in 2024. Despite significant advancements in breast cancer treatment, it continues to pose a major healthcare challenge due to the complexity of underlying mechanisms, including multiple signaling pathways, transcription factors, signal transducers, oncogenes, tumor suppressor genes, and signaling receptors. Current therapeutic strategies for breast cancer include chemotherapy with agents such as paclitaxel, cyclophosphamide, doxorubicin, docetaxel, carboplatin, cisplatin, epirubicin, and bevacizumab; surgical removal of tumors; radiotherapy; hormonal therapy (e.g., tamoxifen, anastrozole); and targeted therapies. However, these approaches are often associated with significant limitations, such as side effects like hair loss, nausea, and weight

*Corresponding Author: Dr. Geeta Singh, Assistant Professor, Department of Biomedical Engineering, DCRUST, Murthal-131039. India. Email: geetasingh.bme@dcrustm.org

Cite as: J. Integr. Sci. Technol., 2025, 13(3), 1062.

URN:NBN:sciencein.jist.2025.v13.1062

DOI:10.62110/sciencein.jist.2025.v13.1062



©Authors CC4-NC-ND, ScienceIN <https://pubs.thesciencein.org/jist>

loss. Additionally, cytotoxic chemotherapy can impair cellular and humoral immunity, making patients more vulnerable to other infections. This necessitates exploring strategies that are both safe and have minimal side effects.

Phytochemicals, natural plant extracts, or derivatives, offer a promising alternative for breast cancer treatment with low toxicity and have shown considerable potential in anticancer applications.¹ These compounds exhibit complementary and synergistic mechanisms that contribute to inhibiting the carcinogenic process by scavenging free radicals², suppressing survival and proliferation of malignant cells³, as well as diminishing invasiveness and angiogenesis of tumors.⁴ They exert a wide and complex range of actions on different molecular targets and signal transduction pathways including membrane receptors, kinases, downstream tumor-activator or -suppressor proteins⁵, transcriptional factors⁶, microRNAs (miRNAs), cyclins, and caspases.⁷

Clinical and pathological factors such as age, lymph node involvement, tumor size, histological grade, hormone receptor status, and HER2 status are routinely used to classify breast cancer patients, aiding prognosis and therapy selection.⁸ Nevertheless, traditional diagnostic methods sometimes fail to accurately predict outcomes in patients with similar profiles, underscoring the need for novel biomarkers to enhance clinical management.

One such promising biomarker is poly(ADP-ribose) polymerase-1 (PARP-1), a widely expressed NAD⁺-dependent nuclear enzyme with prognostic significance in various cancers.⁹ The PARP-1 gene, located on chromosome 1q41–42, consists of 23 exons and spans approximately 47.3 kb. PARP-1 is crucial for catalyzing poly(ADP-ribosyl)ation, a rapid, DNA damage-dependent post-translational modification that impacts itself, histones, and other nuclear proteins. This modification is thought to play a multifaceted role in various cellular processes, including DNA damage recognition and repair, cell death pathways, and mitotic apparatus function.¹⁰

The DNA-binding domain of PARP-1 attaches to DNA-breaks through two zinc finger domains, while its C-terminal catalytic domain sequentially transfers ADP-ribosyl groups (PAR) from nicotinamide adenine dinucleotide (NAD⁺) to chromatin-associated proteins involved in repair.¹¹

By adding poly (ADP-ribose) chains to numerous client proteins, PARP-1 plays a key role in the DNA damage response, base-excision repair, and DNA strand break repair, which are essential for maintaining genomic stability.¹² Additionally, PARP-1 influences chromatin structure and gene regulation. The nuclear enzyme PARP1 is crucial for detecting DNA damage and aiding repair.¹¹ PARP-1 activation occurs through phosphorylation by the hormone-activated cyclin-dependent kinase CDK2 at two consecutive serine residues, which enhances its PARylation activity.¹³

PARP-1 is particularly important in estrogen receptor alpha (ER α)-positive (ER+) breast cancers, where it regulates pathways that drive estrogen-dependent gene expression and cell proliferation.¹⁴ In tumors with BRCA1/2 mutations, PARP1 serves as a crucial alternative DNA repair pathway, and PARP inhibitors can induce synthetic lethality, resulting in cell cycle arrest and apoptosis.¹¹ These inhibitors have been approved for treating

patients with BRCA1/2-mutated breast cancer, leveraging this synthetic lethality mechanism.¹⁵

PARP-targeted therapies have shown promise in BRCA1/2-deficient cancer models, highlighting their therapeutic potential.¹⁶ PARP-1 expression levels serve as a prognostic marker linked to poor survival outcomes, with evidence suggesting a correlation between high PARP-1 expression and tumor treatment resistance.¹⁷ PARP-1 expression is significantly elevated in various malignancies, including breast, uterine, lung, ovarian, and skin cancers, as well as non-Hodgkin's lymphoma.¹⁸ In breast infiltrating ductal carcinoma (IDC), the mean PARP-1 expression is notably higher than in normal breast tissue, with over 30% of IDC samples showing upregulation compared to only 2.9% in normal tissue.¹⁹ This positions PARP-1 inhibitors as potential antitumor agents, capable of enhancing the efficacy of conventional therapies or functioning independently in tumors with impaired DNA repair mechanisms.¹⁵ Research by Domagala *et al.* revealed that most breast carcinomas exhibit high nuclear PARP-1 expression, with a smaller percentage showing nuclear and cytoplasmic expression. They found a strong association between nuclear PARP-1 expression and BRCA1 status in basal-like and triple-negative (TN) breast cancers. This suggests that low PARP-1 expression in certain BRCA1-associated and TN breast cancers may limit the effectiveness of PARP inhibitor therapy.²⁰ In another study, Luo *et al.* were the first to explore the relationship among androgen receptor (AR), PARP-1, and BRCA1 in TNBC, discovering that following BRCA1 overexpression the AR and PARP-1 levels at both mRNA and protein levels decreased. Their *in-vitro* findings demonstrated that AR positively regulates PARP-1, while PARP-1 enhances AR expression. Additionally, they confirmed a negative correlation between BRCA1 expression and both AR and PARP1 in TNBC patients.²¹ Siker *et al.* showed that a sequential combination of PARP and PI3K inhibitors is more effective than PARP inhibition alone in targeting BRCA1-deficient breast cancer cells, highlighting the potential of combination therapies to improve treatment outcomes for patients with specific tumor profiles.²² However, the adverse effects of PARP-1 inhibitors²³ and the development of drug resistance with prolonged treatment highlights the need for discovering new, naturally occurring PARP-1 inhibitors for breast cancer therapy. This study investigated the PARP-1 inhibitory potential of phytochemicals targeting the 7KK6 protein, the crystal structure representing constitutively active PARP-1.

We conducted structure-based *in-silico* screening of 247 phytochemicals. Furthermore, molecular dynamics (MD) simulations were performed on the identified lead compounds to assess the stability of the complexes over 100 ns. Stereochemical analysis and ADME studies were also conducted to further characterize these interactions.

MATERIALS AND METHODOLOGY

Methods and Databases Employed

The crystal structure of the target protein, i.e., PARP-1 (PDB ID: 7KK6), was downloaded from the RCSB website (<https://www.rcsb.org>). The structures of phytochemicals were retrieved from PubChem.²⁴ Docking and molecular dynamics

studies were conducted using the Schrödinger software under an evaluation license valid for November 2023.

Data Collection and Ligand Preparation

A phytochemical library of 247 phytochemicals from various plants was prepared, and their structures were retrieved from PubChem. All these compounds were prepared using the LigPrep tool of the Schrödinger²⁵ suite under physiological pH conditions. The geometry of the ligand was minimized using the OPLS_2005 force field, and the ionization states were defined using the Epik module.²⁶

Protein preparation

The crystal structure of PARP-1 (PDB: 7KK6) was collected from the RCSB protein databank (PDB). The protein structure was prepared by using the Protein Preparation Wizard and Prime module of the Schrodinger suite.²⁷ The protein preparation is a necessary step to make protein structure free from structural, conformational, charge defects and missing atoms at the physiological pH. The study was carried out as per earlier reported literature.²⁸

Preparation of molecular library for virtual screening

In the present study, a compound, Veliparib, already present in crystal structure was considered control (Ct), and molecular docking was performed.²⁹ All parameters were kept default except chirality. The absolute configurations were retained and specified for both Ct and phytochemicals. All ligands were desalted and tautomers were generated. The inbuilt Epik module of the Schrodinger suite was used to estimate ionization states at pH 7 \pm 2 for all compounds.³⁰

Molecular docking studies

The site-specific molecular docking of both Ct and phytochemical library against 7KK6 was performed using the Glide module.³¹ The parameters were kept default for both proteins during receptor grid generation by using Glide. The grid center coordinates for 7KK6 were X= 42.57, Y = 21.25, and Z = 47.07. The size of the cubical grid box was 30 Å. The molecular docking was performed in three steps (HTVS, SP, and XP precision) where only 10% of compounds were passed from each level to the next level. The binding free energy for Ct and top-ranked compounds was also calculated using prime MM/GBSA.³²

Molecular dynamics simulations

Molecular dynamics simulations of the selected docked complexes were performed to retrieve detailed insights into the dynamic behavior of the docked complexes along with the selected control. All the molecular dynamics simulations were carried out in the academic Maestro-Desmond tool³³ with the in-built OPLS-2005 force field.³⁴ Before conducting simulations, the docked complexes were solvated with the TIP3P water model³⁵ in a 10 \times 10 \times 10 Å³ orthorhombic box. The cation (Na⁺) and anion (Cl⁻) were added to neutralize the systems and to maintain the physiological pH. Prior to simulations, all the systems were energetically minimized for 100ps at default conditions. The Martyna–Tobias–Klein and Nose–Hoover chain dynamic algorithms were used to maintain the pressure 1.0 bar and temperature of the systems at 300K, respectively.³⁶ Thereafter, the production run of 100 ns time duration was carried out on the systems. Properties like root-mean-square-deviation (RMSD), root-mean-square-fluctuation (RMSF),

protein-ligand interactions, and contacts were scrutinized to check the stability of the docked complexes. The stereo-chemical geometry of 7KK6 was analyzed after MD simulation by Procheck.³⁷ The Dynamic Cross Correlation Matrix (DCCM) was calculated to analyze the correlated motion of protein residues during MD simulations.

Validation of docking studies

The non-site-specific docking was performed to validate results to illustrate the absence of an allosteric site for our promising molecules. Top-ranked compounds based on glide docking score and XP gscore in site-specific glide docking were further re-screened through non-site specific blind docking using AutodockVina in PyRx (version 0.8)³⁸ as a means of docking validation. In PyRx, the universal force field and the conjugate algorithm were used to minimize all compounds before blind docking. The results were analyzed on the Pymol platform (The PyMOL Molecular Graphics System).³⁹

Absorption, distribution, metabolism, and excretion calculation

The absorption, distribution, metabolism, excretion, and toxicity (ADMET) profiles of promising compounds were calculated by using Swiss ADME.⁴⁰ The predicted ADME properties include molecular weight (MW), HBA, HBD, TPSA (total polar surface area), predicted octanol/water partition coefficient (MLogP), solubility (ESOL class), GI absorption, BBB permeant, cytochrome inhibitor (CYP1A2, CYP2C19, CYP2C9, CYP2D6 and CYP3A4).

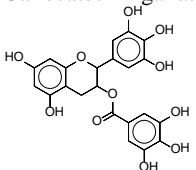
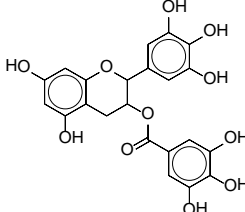
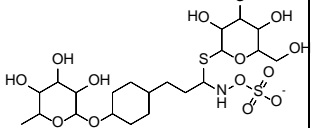
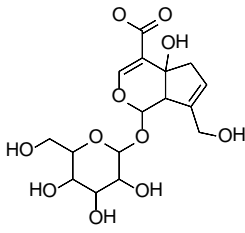
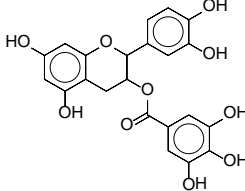
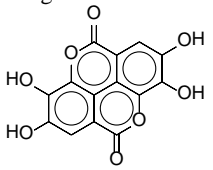
RESULTS AND DISCUSSIONS

Molecular Docking Results of Phytochemicals

Molecular docking calculations were performed to identify phytochemicals that could bind strongly to PARP1 protein using the GLIDE module. Docking score (kcal/mol), and binding free energy (kcal/mol) were considered to rank the poses of the ligands. In the case of PARP1 (PDB ID 7KK6), all 247 phytochemicals were docked within the protein binding pocket. However, based on the docking score (-8.309 kcal/mol), and binding free energy (-67.69 kcal/mol) of control (Ct) (Table 1, entry 9), a total of 28 phytocompounds (Table 1 entry 1-8 and Table 2 entry 1-20) displayed higher docking score than Ct whereas 8 out of 28 showed better binding free energy (Table 1 entry 1-8). Hit compound P1, Gallic acid gallate showed docking score, and binding free energy of -11.574 kcal/mol and 81.28 kcal/mol, respectively (Table 1, entry 1). The remaining 219 compounds showed docking scores lower than that of the control as depicted in Table S1 (Supplementary).

The ligand-protein interaction analysis revealed that the hydroxy group of compound P1 interacted with Glu763, Asn767, Gly863, and Ser864 by H-bond only whereas the phenyl ring interacted with His862, and Tyr907 by pi-pi interaction. There were no salt bridge interactions found. Ct interacted by H-bond (Glu763, Gly863, Ser904), salt bridge interaction (Glu763), pi-pi interaction (Tyr907), and pi-cation interaction (Tyr896) (Figure 1). Both P1 and Ct showed few common interactions with residues Glu763, Gly863, and Tyr907.

Table 1. List of phytochemicals hit molecules based on docking score (kcal/mol), XP Gscore (kcal/mol), and their binding free energy (kcal/mol) towards the targeted 7KK6 protein.

| Entry No. | Code, Name, Structure | Docking score (kcal/mol) | MMGBSA dG Bind (kcal/mol) |
|-----------|--|--------------------------|---------------------------|
| 1 | P1 Gallocatechin gallate  | -11.574 | -81.29 |
| 2 | P2 Epigallocatechin Gallate  | -11.565 | -72.45 |
| 3 | P3 Glucomoringin  | -10.415 | -70.85 |
| 4 | P4 Theveside  | -10.346 | -74.55 |
| 5 | P5 Catechin gallate  | -10.143 | -81.94 |
| 6 | P6 Ellagic Acid  | -9.873 | -69.97 |

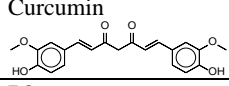
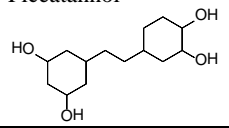
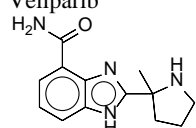
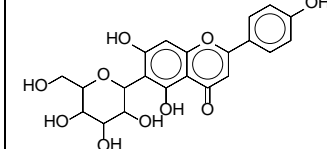
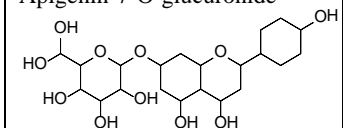
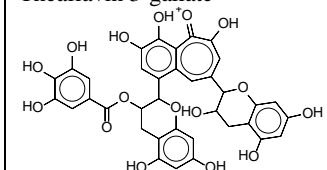
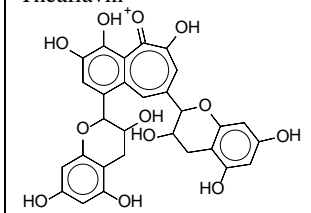
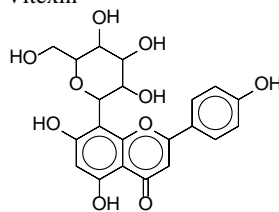
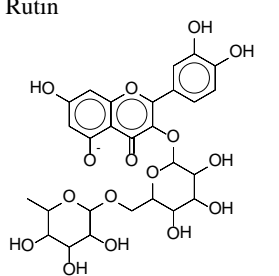
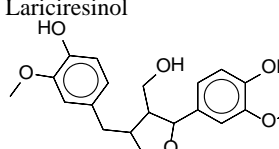
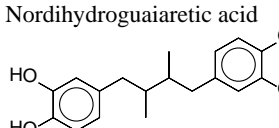
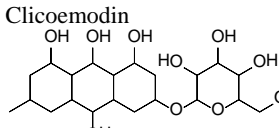
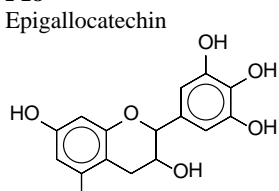
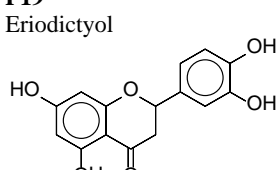
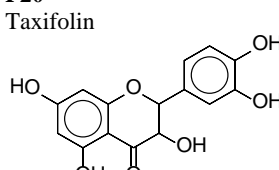
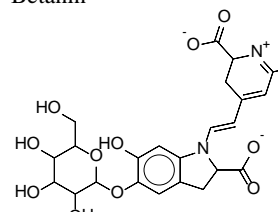
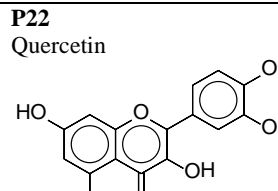
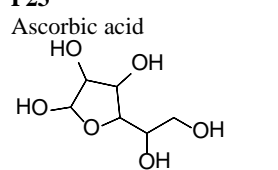
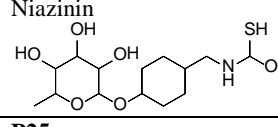
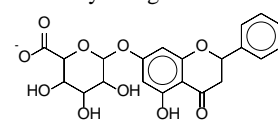
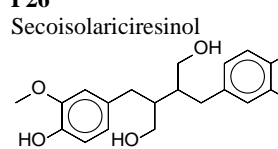
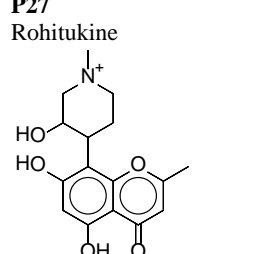
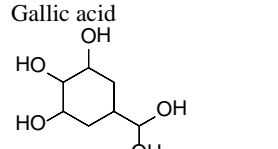
| | | | |
|---|--|--------|--------|
| 7 | P7 Curcumin  | -9.328 | -73.06 |
| 8 | P8 Piceatannol  | -8.575 | -67.97 |
| 9 | Ct Veliparib  | -8.309 | -67.69 |

Table 2. List of phytocompound hit molecules based on docking score (kcal/mol), XP Gscore (kcal/mol), and their binding free energy (kcal/mol) towards the targeted 7KK6 protein.

| Entry No. | Code, Name Structure | Docking score (kcal/mol) | MMGBSA dG Binding energy (kcal/mol) |
|-----------|--|--------------------------|-------------------------------------|
| 1 | P9 Isovitexin  | -11.335 | -62.22 |
| 2 | P10 Apigenin-7-O-glucuronide  | -11.212 | -62.09 |
| 3 | P11 Theaflavin 3-gallate  | -11.174 | -56.90 |
| 4 | P12 Theaflavin  | -9.917 | -66.14 |

| | | | |
|----|---|--------|--------|
| 5 | P13 Vitamin  | -9.794 | -56.31 |
| 6 | P14 Rutin  | -9.748 | -56.49 |
| 7 | P15 Lariciresinol  | -9.441 | -60.04 |
| 8 | P16 Nordihydroguaiaretic acid  | -9.380 | -52.95 |
| 9 | P17 Cliccoemodin  | -9.319 | -66.59 |
| 10 | P18 Epigallocatechin  | -9.087 | -39.18 |
| 11 | P19 Eriodictyol  | -9.069 | -59.75 |
| 12 | P20 Taxifolin  | -8.973 | -56.59 |

| | | | |
|----|---|--------|--------|
| 13 | P21 Betanin  | -8.972 | -31.66 |
| 14 | P22 Quercetin  | -8.942 | -56.66 |
| 15 | P23 Ascorbic acid  | -8.775 | -32.08 |
| 16 | P24 Niazinin  | -8.636 | -65.03 |
| 17 | P25 Eriodictyol-7-glucuronide  | -8.595 | -67.28 |
| 18 | P26 Secoisolariciresinol  | -8.390 | -60.46 |
| 19 | P27 Rohitukine  | -8.357 | -59.07 |
| 20 | P28 Gallic acid  | -8.356 | -48.04 |

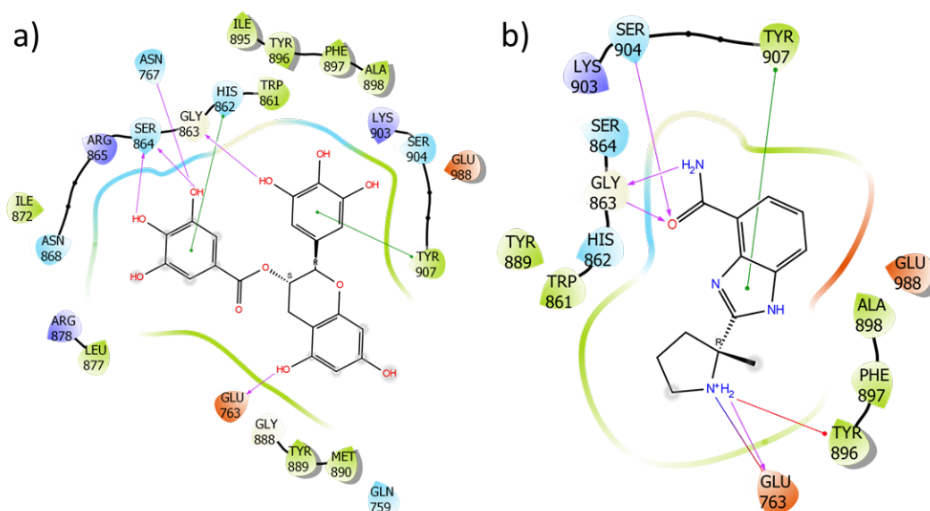


Figure 1. Ligand interaction Diagram, (a) 7KK6-P1, and (b) 7KK6- Ct complexes

Docking validation by non-site-specific docking

Non-site-specific docking performed by PyRx software indicated that both P1 and Ct docked at active sites, suggesting no allosteric site binding for P1 (Figure 2).

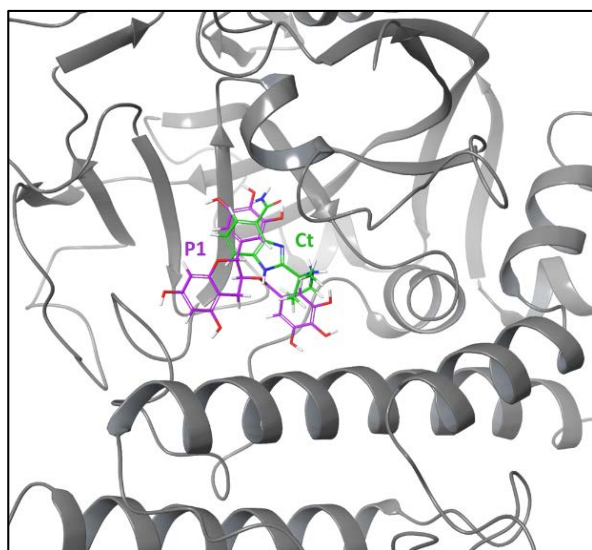


Figure 2: Docking validation for P1 and Ct in complex with 7KK6

Molecular dynamics simulations

Extensive molecular dynamics simulations were carried out for 100ns to study the stability, and the conformational behavior of P1 phytocompound and Ct formed complex with 7KK6 enzyme. The stabilities of the compounds were measured by root mean square deviation (RMSD), root mean square fluctuation (RMSF), and contacts formed during the simulation run.

As 7KK6-P1 (Figure 3) formed a stable complex, the stability of these systems was measured by the root mean square deviation (RMSD) change for protein C α during the simulations. The RMSD

plot of C α -7KK6 in complex with compound P1, and Ct attained stability within the first 5ns and fluctuations were in the acceptable region (3Å) (Figure 3a and 4a). The average values of RMSDC α , for the 7KK6 in complex with compound P1, were 2.16 Å (range 1.246-3.235), and 2.15 Å (range 1.232-3.234 Å). Similarly, RMSDC α , for the 7KK6 in complex with compound Ct were 2.17 (range 1.402-2.814), and 2.18 (range 1.383-2.837 Å). In both complexes, protein RMSDC α was observed to be significantly stable. Thus, indicating that the protein was very stable and compounds were not causing any major conformational change in the protein. Similarly, the protein RMSF plot showed that residues of both 7KK6-P1 and 7KK6-Ct

complexes had lesser fluctuations as well as the binding site residues in both complexes fluctuated below 2 Å further confirming the protein stability (Figure 3b, and 4b).

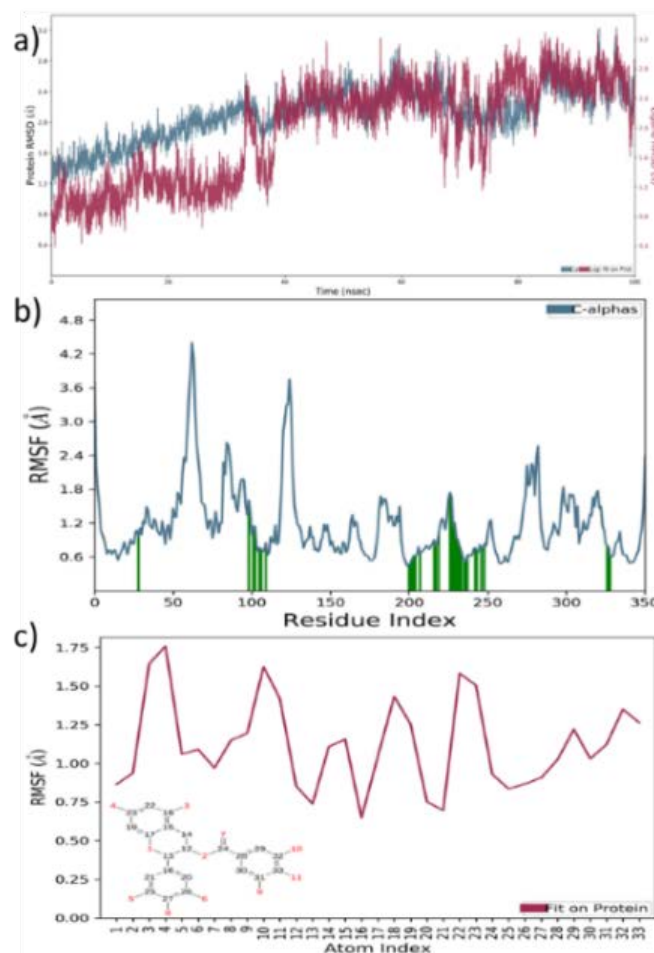


Figure 3. MD simulation results of 7KK6-P1 complex (a) RMSD plot (b) 7KK6 C α RMSF and (c) compound P1 RMSF.

Next, to confirm the stable behavior of the ligand within the binding pocket of 7KK6 protein, ligand-RMSD and ligand-RMSF were calculated. The average ligand RMSD (ligand fit on protein) for compounds P1, and Ct were 2.03Å (range 0.435-3.356 Å), and 0.82Å (range 0.232-1.850 Å), respectively (Figure 3a, and 4a). Linagd-RMSF indicated that both ligands fluctuated below 2 Å signifies that both ligands were very stable during the simulation. (Figure 3c, and 4c).

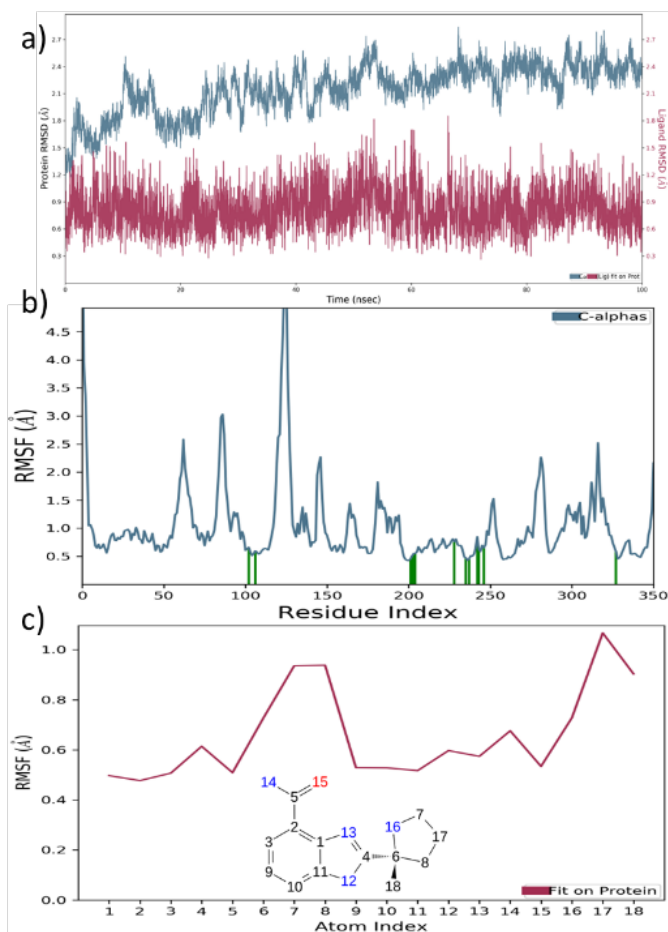


Figure 4. MD simulation results of 7KK6-Ct complex (a) RMSD plot (b) 7KK6 Cα RMSF and (c) compound Ct RMSF.

In addition, the interactions between compound P1 and the binding site residues of 7KK6 were studied as presented in Figure 5a. It was observed that compound P1 was able to maintain interactions with hotspot residues (Asn767, Gly863, Ser864, and Tyr907). It also interacted with Asp770, Gly888, Tyr896, Glu988 (Figure 5a). The compound Ct maintained interactions with the hotspot residues (Glu763, Gly863, Tyr896, Ser904, and Tyr907) and with Glu988 (Figure 5b). Both compounds P1 and Ct interacted with common residues Glu763, Gly863, Tyr896, Ser904, Tyr907, and Glu988. Significant water interactions were involved in compound P1 stability compared to Ct.

Dynamic cross-correlation and principle component analysis for 7KK6

As seen in Figure 6, compound P1 presented decreased

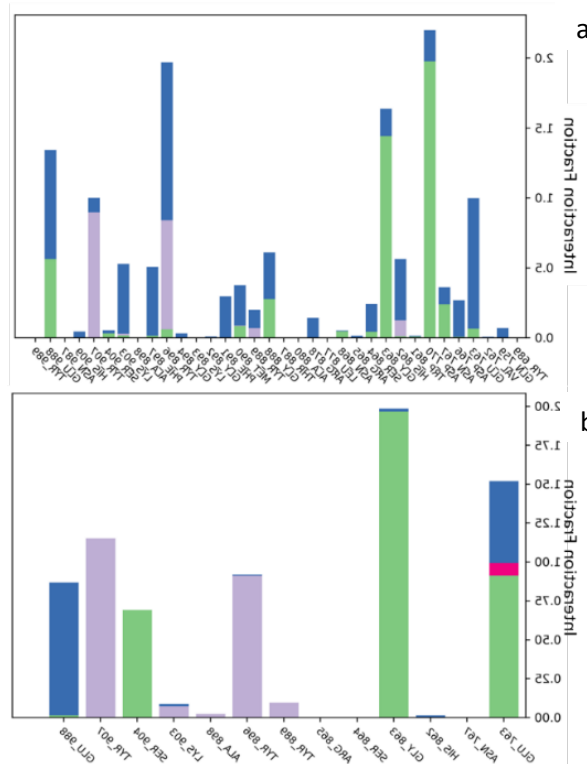


Figure 5: ligand contacts histogram a) 7KK6-P1 complex, and b) 7KK6-Ct complex where H-bond, salt bridge, hydrophobic and water interaction shown by color green, pink, grey, and blue, respectively.

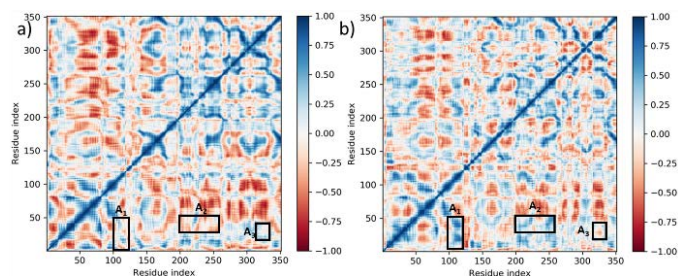


Figure 6: Dynamic cross-correlation a) 7KK6-P1, and b) 7KK6-Ct complexes

correlated movements, notably for residues near the binding site, compared to compound Ct which can be seen in regions A1 and A2 whereas A3 showed increased correlation movements. The correlation change showed that the complex had more fluctuations and residue interactions than Ct. The DCCM analysis suggested a more flexible and less constrained 7KK6-P1 complex as compared to 7KK6-Ct.

MM/GBSA Free Energy Analysis

The MM/GBSA calculations were used to quantitatively elucidate the energetics of compound P1, and Ct binding. The binding free energy (ΔG°) was calculated at an interval of every 2ns for compounds P1, and Ct in complex with 7KK6 (Table 3). As was shown by the MMGBSA analysis, the ΔG° for 7KK6-P1 and 7KK6-Ct complexes was -58.10 ± 7.42 kcal/mol, and -51.18 ± 5.17 kcal/mol, respectively. A lower binding free energy for the 7KK6-P1 complex showed that compound P1 bound more strongly to the binding residues than the Ct.

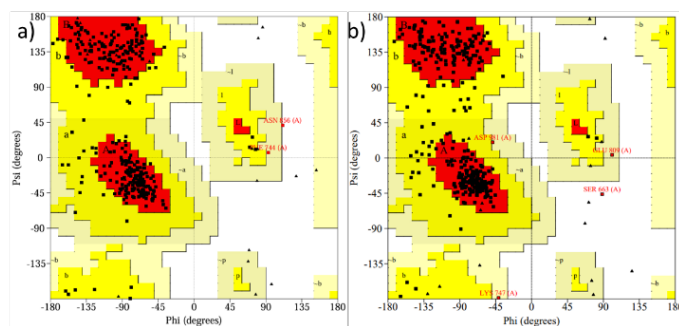
Table 3. Thermodynamic MM/GBSA results for P1 and Ct in complex with 7KK6 for every 2ns

| Time (ns) | P1 ΔG° (kcal/mol) | Ct ΔG° (kcal/mol) |
|-----------|--------------------------------|--------------------------------|
| 6 | -64.59104468 | -55.94903091 |
| 8 | -66.63347245 | -58.20285846 |
| 10 | -68.50760673 | -57.21186262 |
| 12 | -60.26346874 | -55.7878441 |
| 14 | -60.58469401 | -53.9946553 |
| 16 | -62.16936376 | -55.14601192 |
| 18 | -59.45566487 | -52.85592221 |
| 20 | -72.21113593 | -49.81527884 |
| 22 | -63.29322988 | -47.59717993 |
| 24 | -60.82984734 | -49.96874277 |
| 26 | -61.98417749 | -57.81500314 |
| 28 | -61.66456406 | -51.08218474 |
| 30 | -57.04412457 | -41.89421966 |
| 32 | -56.51048957 | -44.00859978 |
| 34 | -51.43792763 | -45.68333607 |
| 36 | -48.20772126 | -49.10540882 |
| 38 | -56.65866757 | -58.07401706 |
| 40 | -51.98777229 | -46.1072655 |
| 42 | -53.66080704 | -49.79018986 |
| 44 | -47.40842348 | -53.34322599 |
| 46 | -60.55244879 | -44.72434111 |
| 48 | -52.09160346 | -46.89300529 |
| 50 | -67.74349988 | -51.53476388 |
| 52 | -62.20993261 | -53.67211822 |
| 54 | -56.8693985 | -51.4942664 |
| 56 | -58.2455159 | -54.64153292 |
| 58 | -67.98726653 | -53.30737234 |
| 60 | -51.54010464 | -48.83556668 |
| 62 | -64.6152282 | -57.12385347 |
| 64 | -61.42164544 | -46.28815239 |
| 66 | -50.12978659 | -43.14054872 |
| 68 | -41.5390035 | -47.47552725 |
| 70 | -60.42073794 | -48.94831863 |
| 72 | -55.51738923 | -58.16193532 |
| 74 | -52.49854574 | -54.19363612 |
| 76 | -68.0575423 | -49.78657443 |
| 78 | -51.82624743 | -56.92694004 |
| 80 | -61.3782006 | -57.72970107 |
| 82 | -70.71231942 | -43.34049308 |
| 84 | -67.18735409 | -47.46918249 |
| 86 | -64.82294689 | -51.28315166 |
| 88 | -59.43236542 | -40.6109472 |
| 90 | -58.49494975 | -41.19725886 |
| 92 | -49.36434697 | -55.75664503 |
| 94 | -46.7289447 | -55.06206919 |
| 96 | -51.92353613 | -53.73125471 |
| 98 | -43.61521221 | -49.38799161 |
| 100 | -46.64848197 | -60.50126401 |

Stereogeometry analysis of 7KK6

The Ramachandran plot of the last frame of 100 ns simulation for both 7KK6-P1 (Asn856) and 7KK6-Ct (Ser663) complexes showed only one residue in the outlier region that indicates good

stereo-chemical geometry of the protein for both the complexes (Figure 7, and Table 4; entry 1-2).

**Figure 7:** Stereogeometry analysis a) P1, and b) Ct**Table 4:** Stereogeometry analysis of 7KK6

| Entry no | Complexes | Favored regions | Additional allowed regions | Generously allowed regions | Disallowed regions |
|----------|-----------|-----------------|----------------------------|----------------------------|--------------------|
| 1 | 7KK6-P1 | 86.1% (267) | 13.2% (41) | 0.3% (1) | 0.3% (1) |
| 2 | 7KK6-Ct | 84.2% (261) | 14.5% (45) | 1.0% (3) | 0.3% (1) |

Ligand properties

Six properties such as ligand RMSD (ligand fit over ligand), the radius of gyration (rGyr), intramolecular H-bond (intraHB), molecular surface area (MolSA), solvent accessible surface area (SASA), and polar surface area (PSA) were analyzed to explain the stability of the compound P1 within 7KK6 receptor complex as shown in Figure 8. Both the compounds P1 and Ct have low ligand RMSD (ligand fit on ligand) compared (below 2 Å) to complex with 7KK6. The radius of gyration was also larger for compound P1 compared to Ct which could be due to the ligand being larger and thus having more flexible regions. Even other parameters were slightly higher for P1 compared to Ct which could be somewhere due to the larger size of P1. Compound P1 didn't show any intramolecular H-bond whereas intramolecular H-bond was shown by Ct.

ADME properties

The ADME profile through SwissADME was calculated for both the compounds P1, and Ct (Table S2, entry 1-2). Compound P1 and Ct were found to have a molecular weight (g/mol) of 458.37, and 244.29, respectively. Both have a TPSA score of above 90 Å² which showed no blood-brain barrier (BBB) penetration capability. Both compounds P1 and Ct showed a water solubility nature but did not show any cytochrome (CYP1A2, CYP2D6, CYP2C19, CYP2C9, and CYP3A4) inhibition. Ct follows the Lipinski rule of 5 as its molecular weight is less than 500, the number of H-bond acceptors (>10), and the number of H-bond donors (>5) whereas P1 does not follow the Lipinski rule of 5 by violating the number of H-bond acceptors (>10) and the number of H-bond donors (>5) parameters.

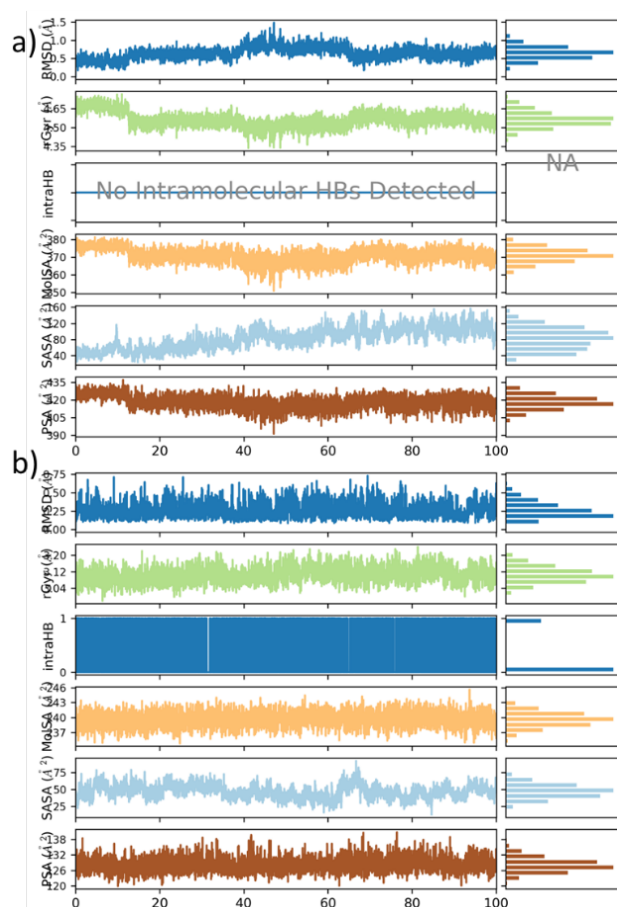


Figure 8: Ligand properties in complex with PARP1 a) P1, and b) Ct

DISCUSSION

The results of this study are in agreement with previous studies demonstrating the therapeutic potential of natural compounds to inhibit PARP-1.⁴¹ As a few examples, PARP-1 binding affinities were found to be significant for both quercetin and resveratrol but with lower binding energies compared to Gallicocatechin gallate. Other molecular dynamics simulations in related studies also emphasized the stability of phytochemical-PARP-1 interactions, which resonates with the robustness of our results.⁴² Perhaps superior performance of Gallicocatechin gallate could be assigned to the structural compatibility that it portrays in the PARP-1 active site, seen by its preferable docking and binding profiles.

In comparison, the clinically approved PARP inhibitor Veliparib shows low efficacy in the metrics of binding energy in our work, also consistent with previous literature pointing toward the balance between efficacy and adverse effects among synthetic inhibitors. With ADME profiling included in the work, it offers a further level of validation that identified lead compounds should exhibit drug-like properties for use in the clinic.

In conclusion, our findings not only confirm but also extend the current understanding of phytochemicals as viable alternatives to synthetic PARP inhibitors. Further *in-vitro* and *in-vivo* studies will be important in further establishing the therapeutic potential of these compounds in clinical settings.

CONCLUSION

In the present work, phytochemicals were virtually screened and their stability within the binding pocket of PARP1 was analyzed by MD simulation for 100ns. A total of 247 phytocompounds were screened against 7KK6. These compounds were ranked based on their docking score and binding free energy better than Ct (-8.309 kcal/mol, -67.69 kcal/mol). 7KK6-P1, and 7KK6-Ct complex were simulated for 100ns. The simulation results indicated that both P1 and Ct compounds were significantly stable. MD simulation supported docking interaction results for both complexes. The ADME profile suggested that P1 doesn't follow lipinski drug-like properties due to a high number of H-bond acceptors and donors. Overall, our results indicate that P1, Gallicocatechin gallate could have a potential role in inhibiting PARP1 in treating breast cancer. Our study requires *in-vitro* evaluations to reveal a promising hope to act as a potential inhibitor of PARP1.

ACKNOWLEDGMENTS

We acknowledge Dr. Prem Prakash Sharma, a research scientist at HeCiT pvt. Ltd's valuable support and guidance during this study.

CONFLICT OF INTEREST STATEMENT

The authors declare no conflict of interest.

SUPPLEMENTARY MATERIAL

A supplementary file accompanying the main article contains additional data and supporting information relevant to the study. For further details, please consult the supplementary file.

AUTHOR CONTRIBUTION

MK was responsible for conceptualization, data curation, drafting the original manuscript, and visualization. BR contributed to conceptualization, supervision, project administration, and the review and editing process. GS oversaw project administration, contributed to supervision, and participated in reviewing and editing the manuscript.

ABBREVIATIONS

| Abbreviation | Full Form |
|--------------|--|
| PARP-1 | Poly(ADP-ribose) polymerase-1 |
| BRCA1/2 | Breast Cancer Gene 1/2 |
| HER2 | Human epidermal growth factor receptor 2 |
| CDK2 | Cyclin-dependent kinase 2 |
| IDC | Infiltrating ductal carcinoma |
| TN | Triple Negative |
| AR | Androgen receptor |
| MD | Molecular dynamic |
| PDB ID | Protein Data Bank ID |
| RCSB | Research collaboratory for structural bioinformatics |
| OPLS | Optimized potentials for liquid simulations |
| XP | Extra precision |
| MMGBSA | Molecular mechanics with generalized born and surface area solvation |
| ADME | Absorption, distribution, metabolism, and excretion |
| TPSA | Total polar surface area |
| MLogP | Moriguchi octanol- water partition coefficient |

| | |
|---------|--|
| BBB | Blood brain barrier |
| GI | Gastrointestinal |
| CYP1A2 | Cytochrome P450 family 1 subfamily A polypeptide 2 |
| CYP2C19 | Cytochrome P450 family 2 subfamily C member 19 |
| CYP2C9 | Cytochrome P450 family 2 subfamily C member 9. |
| CYP2D6 | Cytochrome P450 family 2 subfamily D member 6 |
| CYP3A4 | Cytochrome P450 family 3 subfamily A member 4 |
| RMSD | Root-mean-square deviation |
| RMSF | Root-mean-square-fluctuations |
| HBA | Hydrogen bond acceptors |
| HBD | Hydrogen bond Donors |
| ESOL | Log S (Solubility) |
| iLOGP | Log Po/w |
| rGyr | Radius of gyration |
| MolSA | Molecular surface area |
| SASA | Solvent accessible surface area |
| PSA | Polar surface area |

REFERENCES AND NOTES

1. B.S. Chhikara, K. Parang. Global Cancer Statistics 2022: the trends projection analysis. *Chem. Biol. Lett.* **2023**, 10 (1), 451.
2. W.L. Lee, J.Y. Huang, L.F. Shyr. Phytoagents for cancer management: regulation of nucleic acid oxidation, ROS, and related mechanisms. *Oxid. Med. Cell Longev.* **2013**, 2013925804.
3. X.-B. Yan, T. Xie, S.-D. Wang et al. Apigenin inhibits proliferation of human chondrosarcoma cells via cell cycle arrest and mitochondrial apoptosis induced by ROS generation-an in vitro and in vivo study. *Int. J. Clin. Exp. Med.* **2018**, 11(3), 1615-31.
4. L. Lu, Z. Zhao, L. Liu et al. Combination of baicalein and docetaxel additively inhibits the growth of non-small cell lung cancer in vivo. *TM Mod. Med.* **2018**, 01(03), 213-18.
5. L.S. Adams, S. Phung, N. Yee et al. Blueberry phytochemicals inhibit growth and metastatic potential of MDA-MB-231 breast cancer cells through modulation of the phosphatidylinositol 3-kinase pathway. *Cancer Res.* **2010**, 70(9), 3594-605.
6. W. Zhang, J. Su, H. Xu et al. Dicumarol inhibits PDK1 and targets multiple malignant behaviors of ovarian cancer cells. *PLoS One* **2017**, 12(6), e0179672.
7. X.-B. Yan, T. Xie, S.-D. Wang et al. Apigenin inhibits proliferation of human chondrosarcoma cells via cell cycle arrest and mitochondrial apoptosis induced by ROS generation-an in vitro and in vivo study. *Int. J. Clin. Exp. Med.* **2018**, 11(3), 1615-31.
8. A. Mazzotta, G. Partipilo, S. De Summa et al. Nuclear PARP1 expression and its prognostic significance in breast cancer patients. *Tumour Biol.* **2016**, 37(5), 6143-53.
9. D.D. Singh, A. Parveen, D.K. Yadav. Role of PARP in TNBC: Mechanism of Inhibition, Clinical Applications, and Resistance. *Biomedicine* **2021**, 9(11).
10. M. Alanazi, A.A. Pathan, Z. Abduljaleel et al. Association between PARP-1 V762A polymorphism and breast cancer susceptibility in Saudi population. *PLoS One* **2013**, 8(12), e85541.
11. C.E. Edmonds, M. Makvandi, B.P. Lieberman et al. [(18F)]FluorThanatrace uptake as a marker of PARP1 expression and activity in breast cancer. *Am. J. Nucl. Med. Mol. Imag.* **2016**, 6(1), 94-101.
12. F.Y. Feng, C. Speers, M. Liu et al. Targeted radiosensitization with PARP1 inhibition: optimization of therapy and identification of biomarkers of response in breast cancer. *Breast Cancer Res. Treat.* **2014**, 147(1), 81-94.
13. R.H. Wright, G. Castellano, J. Bonet et al. CDK2-dependent activation of PARP-1 is required for hormonal gene regulation in breast cancer cells. *Genes Dev.* **2012**, 26(17), 1972-83.
14. S.S. Gadad, C.V. Camacho, V. Malladi et al. PARP-1 Regulates Estrogen-Dependent Gene Expression in Estrogen Receptor α -Positive Breast Cancer Cells. *Mol. Cancer Res.* **2021**, 19(10), 1688-98.
15. R. Gong, Z. Ma, L. He et al. Identification and evaluation of a novel PARP1 inhibitor for the treatment of triple-negative breast cancer. *Chem. Biol. Interact.* **2023**, 382110567.
16. M.J. Schiewer, K.E. Knudsen. Transcriptional roles of PARP1 in cancer. *Mol. Cancer Res.* **2014**, 12(8), 1069-80.
17. J. Stanley, L. Klepczyk, K. Keene et al. PARP1 and phospho-p65 protein expression is increased in human HER2-positive breast cancers. *Breast Cancer Res. Treat.* **2015**, 150(3), 569-79.
18. M. Gilabert, S. Launay, C. Ginestier et al. Poly(ADP-Ribose) Polymerase 1 (PARP1) Overexpression in Human Breast Cancer Stem Cells and Resistance to Olaparib. *PLoS ONE* **2014**, 9(8), e104302.
19. V. Ossovskaya, I.C. Koo, E.P. Kaldjian et al. Upregulation of Poly (ADP-Ribose) Polymerase-1 (PARP1) in Triple-Negative Breast Cancer and Other Primary Human Tumor Types. *Genes Cancer* **2010**, 1(8), 812-21.
20. P. Domagala, T. Huzarski, J. Lubinski et al. PARP-1 expression in breast cancer including BRCA1-associated, triple negative and basal-like tumors: possible implications for PARP-1 inhibitor therapy. *Breast Cancer Res. Treat.* **2011**, 127(3), 861-9.
21. J. Luo, J. Jin, F. Yang et al. The Correlation Between PARP1 and BRCA1 in AR Positive Triple-negative Breast Cancer. *Int. J. Biol. Sci.* **2016**, 12(12), 1500-10.
22. S. Kimbung, E. Biskup, I. Johansson et al. Co-targeting of the PI3K pathway improves the response of BRCA1 deficient breast cancer cells to PARP1 inhibition. *Cancer Lett.* **2012**, 319(2), 232-41.
23. C. Wang, J. Li. Haematologic toxicities with PARP inhibitors in cancer patients: an up-to-date meta-analysis of 29 randomized controlled trials. *J. Clin. Pharm. Ther.* **2021**, 46(3), 571-84.
24. S. Kim, J. Chen, T. Cheng et al. PubChem 2023 update. *Nucleic Acids Res.* **2022**, 51(D1), D1373-D80.
25. A. Senrunga, D. Kumar, N. Bhardwaj, et al. Discovery of novel bioactive compounds in Catharanthus roseus exhibiting anti-angiogenic activity against VEGFR-2 TKD for Glioblastoma tumor growth suppression. *Biomed. Ther. Lett.* **2024**, 11 (2), 912.
26. S.I. Khalivulla, U.R.S. Arigala, B.V.K.K. Althurthi. Molecular Docking Studies of 3a,4-dihydro-3H-[1,3,2] oxazaphospholo [3,4-a]Indole-1-oxide derivatives for Anticancer activity. *J. Mol. Chem.* **2024**, 4 (2 SE-Molecular Simulations), 697.
27. V. Rustagi, S.R.R. Gupta, A. Singh, I.K. Singh. Beyond trial and error: Leveraging advanced software for Therapeutic discovery. *Chem. Biol. Lett.* **2025**, 12 (1), 1251.
28. S. Kumar, P.P. Sharma, U. Shankar et al. Discovery of New Hydroxyethylamine Analogs against 3CLpro Protein Target of SARS-CoV-2: Molecular Docking, Molecular Dynamics Simulation, and Structure-Activity Relationship Studies. *J. Chem. Inf. Model.* **2020**, 60(12), 5754-70.
29. K. Madaan, S. Mehta, R. Singh. Structure-Based Virtual Screening, ADMET prediction and Molecular Dynamics simulation of isoindolin-1-one scaffolds as potential inhibitors of MNK2. *Biomed. Ther. Lett.* **2024**, 11 (2), 910.
30. C.B.C. Ikpa, N.N. Chidozie-Ikpa. Molecular docking of phytochemical compounds in Cucurbita maxima with anti-prostate cancer activity. *J. Mol. Chem.* **2024**, 4 (1), 685.
31. A. Das, B. Stany, S. Mishra, et al. Computational insights of Catharanthus roseus phytochemicals against putative proteins of pathogenic Yersinia ruckeri to combat red mouth disease in salmonid fishes. *J. Mol. Chem.* **2024**, 4 (1), 683.
32. Schrödinger Release 2020-1: Prime, Schrödinger, LLC, New York, NY, 2020.
33. Schrödinger Release 2020-1: Desmond Molecular Dynamics System, D. E. Shaw Research, New York, NY, 2020. Maestro-Desmond Interoperability Tools, Schrödinger, New York, NY, 2020.
34. W.L. Jorgensen, D.S. Maxwell, J. Tirado-Rives. Development and Testing of the OPLS All-Atom Force Field on Conformational Energetics and Properties of Organic Liquids. *J. Am. Chem. Soc.* **1996**, 118(45), 11225-36.
35. W.L. Jorgensen, J. Chandrasekhar, J.D. Madura et al. Comparison of simple potential functions for simulating liquid water. *J. Chem. Phys.* **1983**, 79(2), 926-35.
36. S. Nosé. A unified formulation of the constant temperature molecular dynamics methods. *J. Chem. Phys.* **1984**, 81(1), 511-19.
37. R.A. Laskowski, M.W. MacArthur, D.S. Moss, J.M. Thornton. PROCHECK: a program to check the stereochemical quality of protein structures. *J. Appl. Cryst.* **1993**, 26(2), 283-91.
38. S. Dallakyan, A.J. Olson In Chemical Biology: Methods and Protocols, J.E. Hempel, C.H. Williams, C.C. Hong, Eds.; Springer New York: New York, NY, **2015**, pp 243-50.
39. Schrödinger, LLC 2015.
40. A. Daina, O. Michielin, V. Zoete. SwissADME: a free web tool to evaluate pharmacokinetics, drug-likeness and medicinal chemistry friendliness of small molecules. *Sci. Rep.* **2017**, 742717.
41. D.O. Koshkina, N.V. Maluchenko, A.N. Korovina et al. Resveratrol Inhibits Nucleosome Binding and Catalytic Activity of PARP1. *Biomolecules* **2024**, 14(11).
42. A. Tharamelvelyil Rajendran, G. Dheeraj Rajesh, P. Kumar et al. Selection of potential natural compounds for poly-ADP-ribose polymerase (PARP) inhibition in glioblastoma therapy by in silico screening methods. *Saudi Journal of Biological Sciences* **2023**, 30(7), 103698.